Geophysical Research Letters

RESEARCH LETTER
10.1029/2022GL100693

A Realistic Projection of Climate Change in the Upper Atmosphere Into the 21st Century

I. Cnossen[1]

[1]British Antarctic Survey, Cambridge, UK

Key Points:

- The first realistic projection of climate change in the upper atmosphere (100–500 km altitude) for 2015–2070 is presented
- The predicted global mean cooling and decline in thermosphere density for 2015–2070 are about twice as strong as for the past
- The largest changes in the ionosphere are expected in the region of ~50°S–20°N and ~90°–0°W

Correspondence to:

I. Cnossen,
inos@bas.ac.uk

Citation:

Cnossen, I. (2022). A realistic projection of climate change in the upper atmosphere into the 21st century. *Geophysical Research Letters*, *49*, e2022GL100693. https://doi.org/10.1029/2022GL100693

Received 7 AUG 2022
Accepted 20 SEP 2022

Abstract Climate change in the upper atmosphere (~90–500 km altitude) has important impacts on practical applications. To prepare for these, realistic projections of future climate change are needed. The first climate projection up to 500 km altitude is presented here based on a long transient simulation with the whole atmosphere community climate model extension, following Shared Socio-economic Pathway 2–4.5, a moderate emission scenario. Effects of predicted main magnetic field changes and reasonable solar radiative and particle forcings are also included. The predicted global mean cooling in the thermosphere and associated decline in thermosphere density for 2015–2070 are significantly stronger than for the historical period, which is ascribed to the more rapid increase in CO_2 concentration. Trends in global mean ionospheric parameters also increase in magnitude, but there are considerable spatial variations, caused by changes in the Earth's magnetic field. The largest ionospheric changes are expected in the region of ~50°S–20°N and ~90–0°W.

Plain Language Summary Increased greenhouse gas concentrations cause global cooling in the middle and upper atmosphere (~15−500 km altitude), causing this part of the atmosphere to shrink. This reduces the air density in the thermosphere (~90−500 km altitude) and also affects the ionosphere, consisting of the charged particles in the atmosphere. These changes in the climate of the upper atmosphere affect satellite safety and satellite-based measurements. Therefore, we need to know what future changes to expect at high altitudes. We simulated this with a global model of the whole atmosphere (~0−500 km altitude), assuming a moderate scenario of future greenhouse gas and other chemical emissions. Realistic assumptions on main magnetic field changes and variations in solar activity, which also affect the climate of the upper atmosphere, were also included. The predicted global mean cooling in the thermosphere and associated decline in thermosphere density for 2015–2070 are clearly stronger than for the past, which is ascribed to the more rapid increase in CO_2 concentration. Climate change in the ionosphere is also stronger for 2015–2070 than for the past, but varies strongly with location, with the largest changes expected in the region of ~50°S–20°N and ~90°–0°W. These are due to changes in the Earth's magnetic field.

1. Introduction

There is overwhelming evidence that the climate of the upper atmosphere is changing. While the troposphere shows a global warming trend, the middle and upper atmosphere (stratosphere, mesosphere, and thermosphere) have been cooling (e.g., Cnossen, 2012; Laštovička et al., 2006). This cooling results in thermal contraction, resulting in a lowering of ionospheric layers (Bremer et al., 2012; Rishbeth & Roble, 1992) and a reduction in thermosphere density at fixed height (Emmert, 2015; Keating et al., 2000; Weng et al., 2020). The increase in atmospheric CO_2 concentration is thought to be the main driver of the global mean cooling and contraction of the upper atmosphere (e.g., Laštovička et al., 2006), with other trace gases playing a relatively minor role (Qian et al., 2013). The secular variation in the Earth's magnetic field also drives significant long-term trends in the upper atmosphere, in particular in the ionosphere, although these vary strongly with location and largely cancel out in a global average (Cnossen, 2014, 2020; Qian et al., 2021).

Long-term changes in the upper atmosphere have important practical implications. The decline in density reduces atmospheric drag on objects passing through the thermosphere, increasing the lifetime and accumulation rate of space debris (Brown et al., 2021; Lewis et al., 2011). As space debris poses a serious hazard to operational spacecraft due to the risk of collisions, this is a pressing concern for the future exploitation of the low Earth orbit (LEO) environment. Further, certain satellite-based measurements, for instance of sea level, need to be corrected for ionospheric effects and could therefore be affected by long-term changes in the ionosphere, particularly in total electron content (TEC). Any applications of such measurements that require long-term measurement stability,

such as sensitive climate monitoring, require a good understanding of long-term changes in the ionosphere to avoid spurious long-term signals in the data products (Scharroo & Smith, 2010).

To manage and prepare for the effects of long-term changes in the upper atmosphere over the next few decades, realistic projections of the future climate are needed. Future projections of the climate near the surface and up into the middle atmosphere are routinely carried out as part of the efforts of the Intergovernmental Panel on Climate Change, through multi-model assessments of agreed representative concentration pathway (RCP) scenarios or the more recent shared socioeconomic pathways (SSPs) (O'Neill et al., 2016). However, these projections do not extend up to sufficiently high altitudes in the thermosphere and ionosphere to estimate effects on TEC and thermosphere density. Estimates of the future state of the upper atmosphere rely purely on snapshot simulations to investigate the effects of future CO_2 concentrations (e.g., Akmaev & Fomichev, 1998; Brown et al., 2021; Roble & Dickinson, 1989; Qian et al., 2008; H. Liu et al., 2020) or future changes in the Earth's magnetic field (Cnossen & Maute, 2020). Aside from focusing on a single driver of long-term change, these lack realistic solar and geomagnetic activity variations and are therefore somewhat limited in scope.

Here, we take a first step in addressing this problem with a long transient simulation with the whole atmosphere community climate model extension (WACCM-X) up to the year 2070, providing the first long-term projection of the climate of the upper atmosphere. The simulation is a continuation of the WACCM-X simulation used by Cnossen (2020) to analyze long-term trends for the period 1950–2015 and follows a moderate future emission scenario for 2015–2070. A realistic prediction of future changes in the Earth's magnetic field is also included, as well as plausible variations in solar radiative and particle forcings. It therefore offers a much more comprehensive assessment of future long-term trends than any previously published studies. We show that predicted global mean trends in the upper atmosphere are expected to become stronger in the future, consistent with the more rapid increase in atmospheric greenhouse gas concentrations. Main magnetic field changes drive additional changes in the ionosphere, which vary strongly with location. These climatic changes in the upper atmosphere will have important consequences for the build-up of space debris in the LEO environment and may also impact on the long-term stability of satellite-based measurements. The projection presented here offers the first realistic insight in the quantitative long-term changes to expect in the upper atmosphere during the next ∼50 years in order to prepare for these effects.

2. Methodology

2.1. WACCM-X Simulation

WACCM-X 2.0 is part of the community Earth system model (CESM) (Hurrell et al., 2013) release 2.1.0, developed by the National Center for Atmospheric Research (NCAR). WACCM-X extends the standard WACCM, which has a model top at ∼140 km, to an altitude of ∼400–700 km (depending on solar activity levels). WACCM-X 2.0 is described in detail by H.-L. Liu et al. (2018) and references therein. The standard resolution of 1.9° latitude × 2.5° longitude with 126 vertical levels was used.

The simulation analyzed here is an extension of the simulation described by Cnossen (2020), which covered the period 1950–2015, with the full simulation now covering the period 1950–2070. Lower boundary forcings and chemical emissions were specified according to the climate model intercomparison project 6 (CMIP6) historical simulation (Eyring et al., 2016) up to 2015 and followed SSP 2–4.5 (O'Neill et al., 2016) thereafter. This is a "middle of the road" scenario, comparable to RCP 4.5. Sea surface temperatures were prescribed from a coupled atmosphere-ocean simulation with CESM2-WACCM6 (Gettelman et al., 2019). Solar radiative and particle forcings were prescribed based on observations for the historical period and following the reference scenario of the CMIP6 recommendation by Matthes et al. (2017) for the future section of the simulation. The main magnetic field was specified according to the International Geomagnetic Reference Field [IGRF-12; Thébault et al. (2015)] up to 2015 and transitioning to the prediction by Aubert (2015) for the future. The simulation thereby includes all known drivers of long-term change in the upper atmosphere: the increase in CO_2 concentration and other greenhouse gases, changes in ozone-depleting substances, changes in the Earth's magnetic field, and variations in solar and geomagnetic activity levels. The future scenarios adopted for all these drivers are "reasonable," offering a plausible, realistic estimate of the future climate of the upper atmosphere, rather than exploring the extremes of what might be possible.

Figure 1 shows the solar and geomagnetic activity levels used to drive the model, as well as the global mean CO_2 concentration at the surface from 1950 to 2070. These are the main drivers of long-term variations and trends in the global mean thermosphere and ionosphere. In this study, we focus on the period 2015–2070, highlighted

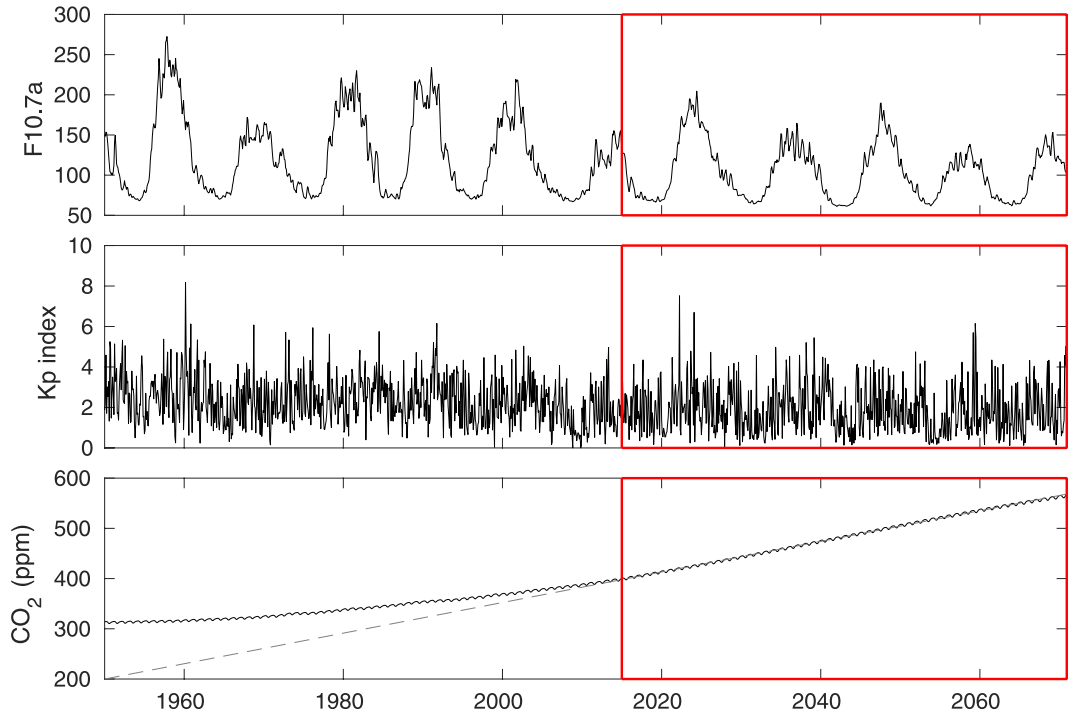

Figure 1. The $F10.7a$ index of solar activity (top), K_P index of geomagnetic activity (middle) and the global mean CO_2 concentration at the surface (bottom) for 1950–2070. Also shown is the linear CO_2 trend calculated for 2015–2070 (dashed gray line), extrapolated backward to show that the CO_2 concentration is increasing more rapidly during 2015–2070 than in the past.

in red in Figure 1. Also shown is the linear CO_2 trend calculated for 2015–2070. This trend is extrapolated backward to show clearly that CO_2 levels are expected to increase more rapidly in the future than in the past: the trend for 2015–2070 is ∼30 ppm/decade under the assumed scenario, which is more than twice the linear trend for 1950–2015 (∼14 ppm/decade). Cnossen and Maute (2020) showed what magnetic field changes are expected from 2015 to 2065 based on the prediction by Aubert (2015), and these are similar for 2015–2070. The largest changes occur in the region of the South Atlantic Anomaly (SAA), where the magnetic field is unusually weak, and the magnetic equator deviates the most from the geographic equator. The SAA is expected to continue to move westwards, intensify, and widen into the future, while the main dipole component is also expected to decrease, at an average rate of ∼27 nT/decade (Aubert, 2015).

2.2. Data Analysis

The analysis uses monthly mean outputs for 2015–2070. Global means were calculated using a cosine (latitude) weighting. While the model uses a vertical pressure coordinate, observational analyses are usually done with reference to geometric height, and therefore, model outputs analyzed here were interpolated to geometric height. Where data were not available up to 500 km altitude, data were extrapolated up to this altitude. Standard linear interpolation/extrapolation was used, although for the neutral and electron density this was done in log-space.

Long-term trends for the period 2015–2070 were calculated by fitting the data to the following linear regression model:

$$Y = a + b \times F10.7a + c \times (F10.7a)^2 + d \times K_p + e \times year \quad (1)$$

where Y is the variable of interest, for example, the global mean mass density at 400 km altitude, $F10.7a$ is the 81-day average of the $F10.7$ index, K_P is the K_P index of geomagnetic activity, and a, b, c, d and e are coefficients to be fitted, with e corresponding to the long-term trend. This regression model was identified by Cnossen (2020) to give the best results for the period 1950–2015 (their model 3). To check for and potentially reduce any remaining solar cycle influences further, average trends for the 11 periods starting in January 2015 and ending between December 2060 and December 2070 (each subsequent period being 12 months longer than the last) were also

Table 1
Mean Trends per Decade for 1950 to 1997–2007 (± Standard Deviation) From Cnossen (2020), Predicted Trends per Decade (± Standard Errors) for 2015–2070, and Mean Trends per Decade for 2015 to 2060–2070 (± Standard Deviation) for the Global Mean Neutral Temperature (T) and Density (ρ) at 400 km Altitude, h_mF_2, N_mF2, and TEC

Variable	Trend (1950 to 1997–2007)	Trend (2015–2070)	Trend (2015 to 2060–2070)
T [K] at 400 km	−3.3 ± 0.4	−5.7 ± 0.7	−6.1 ± 0.5
ρ [%] at 400 km	−2.4 ± 0.3	−6.1 ± 0.8	−5.8 ± 0.4
h_mF_2 [km]	−1.2 ± 0.1	−1.6 ± 0.1	−1.7 ± 0.1
N_mF_2 [%]	−0.5 ± 0.1	−2.0 ± 0.3	−1.9 ± 0.1
TEC [TECU]	−0.19 ± 0.03	−0.29 ± 0.05	−0.28 ± 0.02

computed, again following Cnossen (2020). Where trends are reported as a percentage per decade, this was calculated relative to the average value over the full time span for which the absolute trend was calculated.

3. Global Mean Trends

Table 1 gives an overview of the predicted trends (± standard error) for 2015–2070 in the same thermosphere-ionosphere parameters as studied by Cnossen (2020). Their average trends for 1950 to 1997–2007 (± standard deviation) are also given for comparison. This period was chosen rather than the full 1950–2015 interval, as Cnossen (2020) showed that solar cycle influences were not properly removed when data for the deep solar minimum of 2008/2009 were included. To test for appropriate removal of solar cycle effects here, average trends for the periods starting in 2015 and ending between 2060 and 2070 were calculated (also shown in Table 1). The standard deviations of the predicted trend values for 2015 to 2060–2070 are smaller or the same as the standard error associated with the fit to the linear regression model for 2015–2070 and the average trends for 2015 to 2060–2070 agree with the trends computed for 2015–2070. This indicates that solar cycle influences are removed quite well with the standard linear regression approach and it also means that the calculated trends would likely have been similar if a different solar forcing had been used, unless, perhaps, an extreme scenario had been adopted.

Compared to the historical trends, the predicted global mean trends in thermosphere temperature and density at 400 km altitude are around a factor 2 larger for 2015–2070, while the trend in global mean N_mF_2 is as much as a factor 3 larger. Predicted trends in global mean h_mF_2 and TEC show a more moderate increase relative to the historical period. Given that the linear trend in CO_2 concentration is about a factor 2 larger for 2015–2070 compared to 1950–2015, the factor 2 difference in the magnitude of global mean trends in thermosphere temperature and density can be fully ascribed to the more rapid increase in CO_2 concentration expected for the future. In the ionosphere, main magnetic field changes play a relatively more important role, which likely explains why future trends in ionospheric parameters are larger by either more than a factor two (N_mF_2) or less (h_mF_2 and TEC).

Figure 2 compares the vertical trend profiles for the global mean neutral temperature and density and the global mean electron density for the historical period (mean trend for 1950 to 1997–2007) and the future (mean trend for 2015 to 2060–2070). The temperature trends for both the past and future periods increase rapidly with height in the lower thermosphere but stabilize above ~300 km altitude. The neutral density trends for the past and future periods appear to show somewhat different vertical profiles, but these differences are probably not significant, given the uncertainty in the trend estimates (not shown, but see Table 1 for errors at 400 km altitude). The electron density trend profiles show a positive trend in the lower ionosphere, up to 200–280 km altitude, with a negative trend at higher altitudes. To help visualize what this means for the global mean electron density profile, Figure 3 shows these evaluated for 1950, 2015, and 2070, assuming $F10.7 = 120$ and $K_P = 2.0$, based on the linear regression model fits. The peak electron density (N_mF_2) is gradually decreasing, together with a lowering of the height of the peak, h_mF_2, while the electron density below the F_2 peak slightly increases.

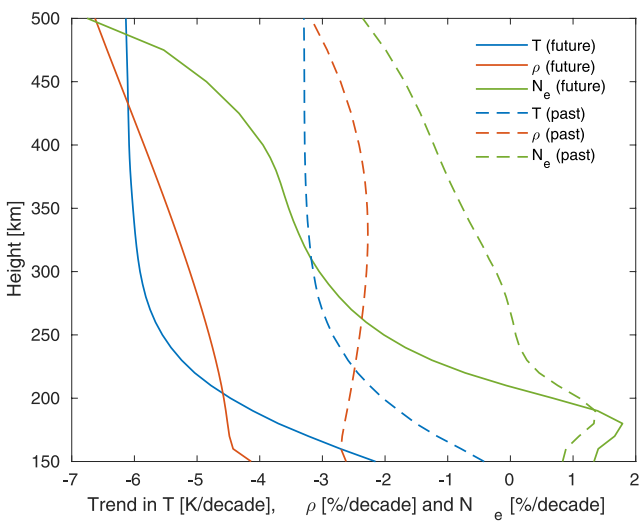

Figure 2. Average trends in global mean temperature (T) [K/decade], neutral density (ρ) [%/decade], and electron density (N_e) [%/decade] for the past (average trend for 1950 to 1997–2007; dashed lines) and for the future (2015–2060–2070; solid lines) as a function of height.

4. Spatial Patterns of Trends

Spatial variations of the long-term trend in thermosphere temperature and density for 2015–2070 (not shown) are similar in nature to those of the trends for 1950–2015. Thermosphere cooling is strongest in the auroral regions, especially in the northern hemisphere, while the reduction in thermosphere density is spatially quite uniform. Cnossen (2020) showed that the stronger cooling trends in the auroral regions can be explained by changes in Joule heating, due to the movement of the magnetic poles.

Spatial patterns of trends in ionospheric parameters are also quite similar for the past and future sections of the simulation, but these spatial variations

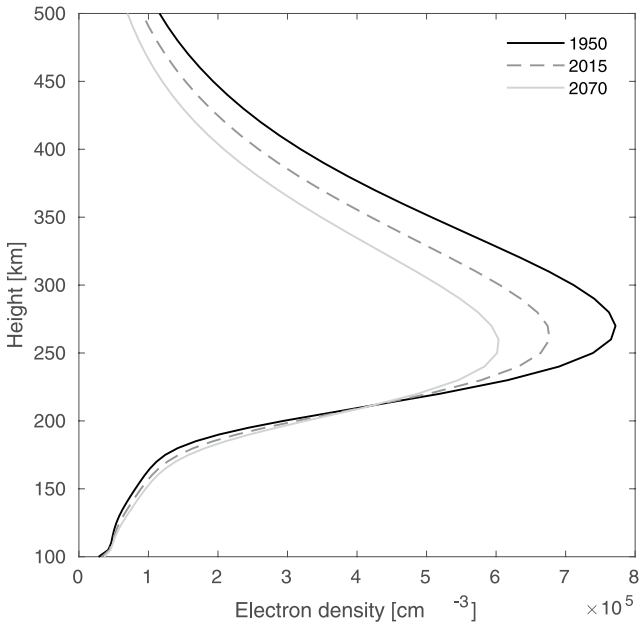

Figure 3. Global mean electron density profiles evaluated for 1950, 2015, and 2070, assuming $F10.7 = 120$ sfu and $K_P = 2.0$.

are much larger. Figure 4 shows a map of the expected trends in total electron content (TEC) for 2015–2070. The strongest changes are expected over South America, the southern Atlantic Ocean, and western Africa, roughly in the region of ~50°S–~20°N and ~90 − 0°W. This is 20–30° further west than the region that had the strongest ionospheric trends for 1950–2015 (Cnossen, 2020). This makes sense, as these large changes are primarily caused by the secular variation of the Earth's magnetic field, which in this area is strongly affected by the westward movement of the SAA. The region also corresponds quite well to that identified by Cnossen and Maute (2020) as having the largest response to expected main magnetic field changes from 2015 to 2065. Cnossen and Maute (2020) further showed some weak effects in the auroral regions, which we see here as well. These auroral changes in TEC are therefore also likely to be driven primarily by changes in the Earth's magnetic field. However, in other parts of the world, the increase in CO_2 concentration probably plays a more important role, causing a negative trend in peak electron density and TEC (e.g., Qian et al., 2021).

In some areas, CO_2 and main magnetic field effects may add up to result in a particularly strong trend. This is likely to be the case over Brazil, where we find an especially large negative trend of up to −1 TECU/decade. However, in other locations the two effects oppose each other and therefore (partly) cancel each other out, resulting in a weaker trend or no significant trend. For example, Cnossen and Maute (2020) showed that predicted main magnetic field changes from 2015 to 2065 cause a significant increase in TEC over Jicamarca (12.0°S, 76.9°W), while we find a moderate negative trend of about −0.3 TECU/decade at this location. This indicates that the effect of the increased CO_2 concentration is stronger over Jicamarca, canceling out the effect of main magnetic field changes, although a stronger negative trend would presumably have occurred if magnetic field effects had not been included. We note that Cnossen and Maute (2020) also found considerable local time variations in trend magnitude, with the strongest trends typically occurring in the afternoon. We are not able to examine such variations here, as only monthly mean data are available. Any local time variations are averaged out.

5. Summary and Conclusions

A long transient simulation with WACCM-X from 1950 to 2070 was conducted, including all known contributing drivers of long-term change in the upper atmosphere: the increase in atmospheric greenhouse gases, changes in ozone-depleting substances, the secular variation of the Earth's magnetic field, and plausible solar and geomagnetic activity variations. For 2015–2070 a moderate emission scenario (SSP2-4.5) was assumed, the magnetic

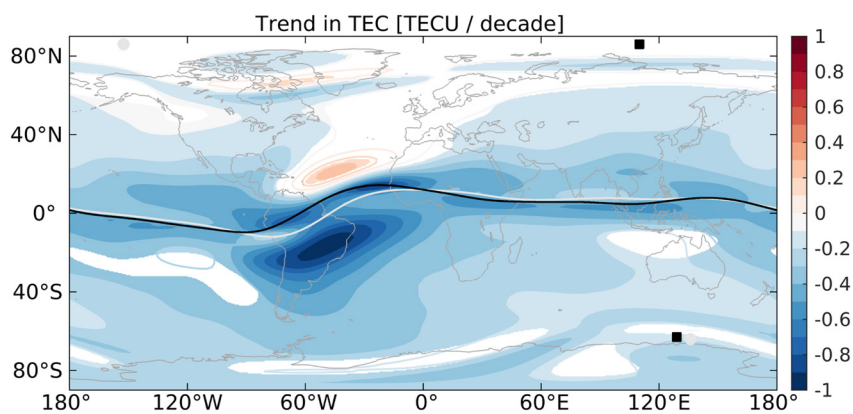

Figure 4. Spatial pattern of trends in TEC (TECU/decade) for 2015–2070. Filled in contours indicate statistical significance at the 95% level based on a two-sided *t*-test, where the null hypothesis is that the trend is zero. The location of the magnetic dip poles and magnetic equator in 2015 (2070) are marked with gray dots (black squares) and a gray (black) line, respectively.

field was specified according to the prediction by Aubert (2015), and solar radiative and particle forcings were prescribed based on the CMIP6 recommendation by Matthes et al. (2017).

Compared to the historical trends, the predicted global mean trends in key thermosphere and ionosphere parameters for 2015–2070 are all significantly larger. Global mean trends in thermosphere density and temperature for 2015–2070 are about twice as large as for the historical period, which can be attributed to the more rapid increase in CO_2 concentration. Predicted temperature trends increase rapidly with height in the lower thermosphere, but stabilize above ∼300 km altitude, while predicted density trends increase more gradually with height throughout the thermosphere. Global mean ionospheric trends for 2015–2070 are either more than a factor 2 (N_mF_2) or noticeably less than a factor 2 (h_mF_2 and TEC) larger than for the historical period, which is likely due to the combined effects of CO_2 and main magnetic field changes. The global mean electron density increases in the F_2 peak region and above, but due to the lowering of the entire electron density profile, an increase in global mean electron density is predicted below ∼220 km altitude.

The global mean decline in thermosphere density is a concern for the future exploitation of the LEO environment due to its impact on atmospheric drag and the lifetime of space debris. The density trend at 400 km altitude predicted for the period 2015–2070 amounts to a total reduction during this time of about 30%–35%. Brown et al. (2021) estimated that a reduction in thermosphere density at 400 km of around 30% would increase orbital lifetimes by about 30% as well. With debris remaining in orbit for longer, the risk of collisions with active satellites or other debris increases, and when a collision occurs, this results in even more fragments, exacerbating the problem. In a follow-up study, we will investigate in more detail how the predicted decline in thermosphere density will affect the space debris environment and the risk of collisions. Further work exploring a wider range of greenhouse gas emission scenarios will also be needed to gain a fuller understanding of the range of conditions we may expect in the upper atmosphere during the next 50–100 years and assess their impact on the LEO environment.

Long-term changes in TEC and the electron density distribution also have practical impacts, for example, on the long-term stability of satellite-based sea level measurements, used for sensitive climate monitoring. However, in this case it is also important to consider the spatial variations, as local/regional trends can be very different from the global mean. This is due to the influence of the secular variation of the Earth's magnetic field, which causes especially large long-term changes in the ionosphere in the region of the SAA. The largest changes in TEC, of up to −1 TECU/decade, are expected to occur over South America, mainly over Brazil. However, relatively large changes, with considerable local structure, can be expected throughout the region of ∼50°S–∼20°N and ∼90° − 0°W. Andima et al. (2019) recently reported on trends in TEC in the African low-latitude region, confirming strong spatial variations in trends, largely organized by the magnetic field. Further studies monitoring the long-term changes in TEC in the region most affected by main magnetic field changes, that is, also over the Southern Atlantic ocean and South America, will be important to help build up a picture of the spatial structure of long-term changes in TEC and control for any effects on satellite-based data applications that require long-term measurement stability.

Data Availability Statement

WACCM-X is part of the Community Earth System Model (CESM). Instructions on how to download the model can be found here: https://www.cesm.ucar.edu/models/cesm2/release_download.html. Monthly mean output data from the WACCM-X simulation presented here for 2015–2070 are publicly available through the Centre for Environmental Data Analysis (CEDA), at: https://catalogue.ceda.ac.uk/uuid/45283390b97c4a27861d74b3d915b0bd and for 1950–2015 at: https://doi.org/10.5285/dc91f5e39ae34fd883af81dfdbaf659c.

Acknowledgments
I. Cnossen was supported by a Natural Environment Research Council (NERC) Independent Research Fellowship (NE/R015651/1). M. Mills and S. Solomon offered initial discussions and advice on the WACCM-X simulation setup and F. Vitt and S. Solomon helped with technical issues in running the model. M. Mills and C. Hannay kindly supplied the sea surface temperature data. Two anonymous reviewers provided thoughtful comments that helped to strengthen the original manuscript. The WACCM-X simulations were run on the ARCHER UK National Supercomputing Service (http://www.archer.ac.uk).

References

Akmaev, R. A., & Fomichev, V. (1998). Cooling of the mesosphere and lower thermosphere due to doubling of CO_2. *Annales Geophysicae*, *16*(11), 1501–1512. https://doi.org/10.1007/s00585-998-1501-z

Andima, G., Amabayo, E. B., Jurua, E., & Cilliers, P. J. (2019). Modeling of GPS total electron content over the african low-latitude region using empirical orthogonal functions. *Annales Geophysicae*, *37*(1), 65–76. https://doi.org/10.5194/angeo-37-65-2019

Aubert, J. (2015). Geomagnetic forecasts driven by thermal wind dynamics in the Earth's core. *Geophysical Journal International*, *203*(3), 1738–1751. https://doi.org/10.1093/gji/ggv394

Bremer, J., Damboldt, T., Mielich, J., & Suessmann, P. (2012). Comparing long-term trends in the ionospheric F2-region with two different methods. *Journal of Atmospheric and Solar-Terrestrial Physics*, *77*, 174–185. https://doi.org/10.1016/j.jastp.2011.12.017

Brown, M. K., Lewis, H. G., Kavanagh, A. J., & Cnossen, I. (2021). Future decreases in thermospheric neutral density in low Earth orbit due to carbon dioxide emissions. *Journal of Geophysical Research: Atmospheres*, *126*(8). https://doi.org/10.1029/2021jd034589

Cnossen, I. (2012). Climate change in the upper atmosphere. In G. Liu (Ed.), *Greenhouse gases – emission, measurement and management*, (pp. 315–336). InTech. https://doi.org/10.5772/32565

Cnossen, I. (2014). The importance of geomagnetic field changes versus rising CO_2 levels for long-term change in the upper atmosphere. *Journal of Space Weather and Space Climate*, *4*, A18. https://doi.org/10.1051/swsc/2014016

Cnossen, I. (2020). Analysis and attribution of climate change in the upper atmosphere from 1950 to 2015 simulated by WACCM-X. *Journal of Geophysical Research: Space Physics*, *125*(12). https://doi.org/10.1029/2020ja028623

Cnossen, I., & Maute, A. (2020). Simulated trends in ionosphere-thermosphere climate due to predicted main magnetic field changes from 2015 to 2065. *Journal of Geophysical Research: Space Physics*, *125*(3). https://doi.org/10.1029/2019ja027738

Emmert, J. T. (2015). Altitude and solar activity dependence of 1967-2005 thermospheric density trends derived from orbital drag. *Journal of Geophysical Research: Space Physics*, *120*(4), 2940–2950. https://doi.org/10.1002/2015ja021047

Eyring, V., Bony, S., Meehl, G. A., Senior, C. A., Stevens, B., Stouffer, R. J., & Taylor, K. E. (2016). Overview of the coupled model intercomparison project phase 6 (CMIP6) experimental design and organization. *Geoscientific Model Development*, *9*(5), 1937–1958. https://doi.org/10.5194/gmd-9-1937-2016

Gettelman, A., Mills, M. J., Kinnison, D. E., Garcia, R. R., Smith, A. K., Marsh, D. R., & Randel, W. J., (2019). The whole atmosphere community climate model version 6 (WACCM6). *Journal of Geophysical Research: Atmospheres*, *124*(23), 12380–12403. https://doi.org/10.1029/2019jd030943

Hurrell, J. W., Holland, M. M., Gent, P. R., Ghan, S., Kay, J. E., Kushner, P. J., et al. (2013). The community Earth system model: A framework for collaborative research. *Bulletin of the American Meteorological Society*, *94*(9), 1339–1360. https://doi.org/10.1175/bams-d-12-00121.1

Keating, G. M., Tolson, R. H., & Bradford, M. S. (2000). Evidence of long term global decline in the Earth's thermospheric densities apparently related to anthropogenic effects. *Geophysical Research Letters*, *27*(10), 1523–1526. https://doi.org/10.1029/2000gl003771

Laštovička, J., Akmaev, R. A., Beig, G., Bremer, J., & Emmert, J. T. (2006). Global change in the upper atmosphere. *Science*, *314*(5803), 1253–1254. https://doi.org/10.1126/science.1135134

Lewis, H. G., Saunders, A., Swinerd, G., & Newland, R. J. (2011). Effect of thermospheric contraction on remediation of the near-Earth space debris environment. *Journal of Geophysical Research*, *116*(A2). https://doi.org/10.1029/2011ja016482

Liu, H., Tao, C., Jin, H., & Nakamoto, Y. (2020). Circulation and tides in a cooler upper atmosphere: Dynamical effects of CO_2 doubling. *Geophysical Research Letters*, *47*(10). https://doi.org/10.1029/2020gl087413

Liu, H.-L., Bardeen, C. G., Foster, B. T., Lauritzen, P., Liu, J., Lu, G., et al. (2018). Development and validation of the whole atmosphere community climate model with thermosphere and ionosphere extension (WACCM-x 2.0). *Journal of Advances in Modeling Earth Systems*, *10*(2), 381–402. https://doi.org/10.1002/2017ms001232

Matthes, K., Funke, B., Andersson, M. E., Barnard, L., Beer, J., Charbonneau, P., et al. (2017). Solar forcing for CMIP6 (v3.2). *Geoscientific Model Development*, *10*(6), 2247–2302. https://doi.org/10.5194/gmd-10-2247-2017

O'Neill, B. C., Tebaldi, C., van Vuuren, D. P., Eyring, V., Friedlingstein, P., Hurtt, G., et al. (2016). The scenario model intercomparison project (ScenarioMIP) for CMIP6. *Geoscientific Model Development*, *9*(9), 3461–3482. https://doi.org/10.5194/gmd-9-3461-2016

Qian, L., Marsh, D., Merkel, A., Solomon, S. C., & Roble, R. G. (2013). Effect of trends of middle atmosphere gases on the mesosphere and thermosphere. *Journal of Geophysical Research: Space Physics*, *118*(6), 3846–3855. https://doi.org/10.1002/jgra.50354

Qian, L., McInerney, J. M., Solomon, S. S., Liu, H., & Burns, A. G. (2021). Climate changes in the upper atmosphere: Contributions by the changing greenhouse gas concentrations and Earth's magnetic field from the 1960s to 2010s. *Journal of Geophysical Research: Space Physics*, *126*(3). https://doi.org/10.1029/2020ja029067

Qian, L., Solomon, S. C., Roble, R. G., & Kane, T. J. (2008). Model simulations of global change in the ionosphere. *Geophysical Research Letters*, *35*(7). https://doi.org/10.1029/2007gl033156

Rishbeth, H., & Roble, R. (1992). Cooling of the upper atmosphere by enhanced greenhouse gases — Modelling of thermospheric and ionospheric effects. *Planetary and Space Science*, *40*(7), 1011–1026. https://doi.org/10.1016/0032-0633(92)90141-a

Roble, R. G., & Dickinson, R. E. (1989). How will changes in carbon dioxide and methane modify the mean structure of the mesosphere and thermosphere? *Geophysical Research Letters*, *16*(12), 1441–1444. https://doi.org/10.1029/gl016i012p01441

Scharroo, R., & Smith, W. H. F. (2010). A global positioning system-based climatology for the total electron content in the ionosphere. *Journal of Geophysical Research*, *115*(A10). https://doi.org/10.1029/2009ja014719

Thébault, E., Finlay, C. C., Beggan, C. D., Alken, P., Aubert, J., Barrois, O., et al. (2015). International geomagnetic reference field: The 12th generation. *Earth Planets and Space*, *67*(1). https://doi.org/10.1186/s40623-015-0228-9

Weng, L., Lei, J., Zhong, J., Dou, X., & Fang, H. (2020). A machine-learning approach to derive long-term trends of thermospheric density. *Geophysical Research Letters*, *47*(6). https://doi.org/10.1029/2020gl087140